



Reevaluation of C₄H Abundance Based on the Revised Dipole Moment

Takahiro Oyama¹ , Hironori Ozaki², Yoshihiro Sumiyoshi², Mitsunori Araki¹ , Shuro Takano³ , Nobuhiko Kuze⁴, and Koichi Tsukiyama¹

¹ Department of Chemistry, Faculty of Science Division I, Tokyo University of Science, 1-3 Kagurazaka, Shinjuku-ku, Tokyo, 162-8601, Japan
t3.oyama@gmail.com

² Division of Pure and Applied Science, Graduate School of Science and Technology, Gunma University, 4-2 Aramaki, Maebashi, Gunma, 371-8510, Japan

³ Department of Physics, General Studies, College of Engineering, Nihon University, 1 Nakagawara, Tokusada, Tamuramachi, Koriyama, Fukushima, 963-8642, Japan

⁴ Department of Materials and Life Sciences, Faculty of Science and Technology, Sophia University, 7-1 Kioi-cho, Chiyoda-ku, Tokyo, 102-8554, Japan

Received 2019 April 24; revised 2019 December 16; accepted 2020 January 8; published 2020 February 11

Abstract

Abnormally large column densities of the carbon-chain molecule, C₄H, have been reported in various sources. The main reason for this was supposed to be an underestimated value of the permanent dipole moment of C₄H. C₄H has a low-lying electronic excited state of ²Π with a large dipole moment in the previous quantum chemical calculations. However, the mixing of the excited state with the ground state ²Σ⁺ has not been taken into consideration. In the present study, we evaluated this mixing by introducing a multireference configuration interaction. The effective dipole moment of C₄H in the ground state was calculated to be 2.10 D, which is about 2.4 times larger than the values used so far. Revised column densities of C₄H in dark clouds, low-mass star-forming regions, and the circumstellar envelope IRC+10216 based upon the new value are about a factor of 6 smaller than the previous values. With the revised column densities, exponential smooth decreases are found for the abundances of the C_{2n}H (*n* = 1–4) molecules with carbon-chain length in these sources, suggesting high similarities among individual formation mechanisms of the C_{2n}H molecules.

Unified Astronomy Thesaurus concepts: Astrochemistry (75); Abundance ratios (11); Interstellar molecules (849); Circumstellar envelopes (237); Star forming regions (1565); Interstellar clouds (834)

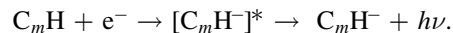
1. Introduction

The carbon-chain series C_{*m*}H (*m* = 2–8) are an essential bench mark of theoretical studies for interstellar chemical reaction networks (e.g., Hassel et al. 2008). Various formation pathways of carbon-chain molecules have been proposed. In the case of C₄H, neutral–neutral reactions (Hasegawa et al. 1992; Smith et al. 2004; Canosa et al. 2007) and ion–neutral reactions starting from various precursors (e.g., Herbst & Leung 1989; Sakai et al. 2013) have been suggested. For example, in the cyanopolyne peak of Taurus Molecular Cloud-1 (TMC-1 CP), the ion–neutral reactions related to the C₄H₂⁺ molecule were thought to be involved in the C₄H formation (Sakai et al. 2013). Formations of longer carbon-chain molecules generated from basic chemical species need more reaction steps than those of shorter ones. Hence, the abundances of the C_{*m*}H molecules in a source are expected to show a gradual decrease along with the increase of the carbon-chain length regardless of whether the neutral–neutral or ion–neutral reactions.

The C_{*m*}H molecules have been observed in dark clouds, star-forming regions, and circumstellar envelopes. Only for C₄H, however, the reported column densities were abnormally large compared with results of reaction network calculations (e.g., Hassel et al. 2008). In the carbon-chain rich sources TMC-1 CP and the circumstellar envelope IRC+10216, the column densities of C₄H are comparable to those of C₂H and are two orders of magnitude larger than those of C₆H (Suzuki et al. 1986; Cernicharo et al. 1987, 2000; Saito et al. 1987). For example, the column densities of the ground vibrational state of the C_{*m*}H (*m* = 2–8) molecules in IRC+10216 are shown in Figure 1. The column density of C₄H deviates significantly from a trend of C₂H, C₆H, and C₈H in this region, although

~1/7 and 1/12 of the total column density of C₄H are distributed to the vibrationally excited states of 1ν₇ and 2ν₇, respectively (Cernicharo et al. 2000). Suzuki et al. (1986) suggested that remarkable differences between the column densities of C₄H and C₆H are due to differences of their reactivities in the electronic ground state, where C₂H and C₄H have the electronic ground states of ²Σ⁺ while C₆H (Suzuki et al. 1986) and C₈H (Woon 1995) have ²Π.

The C_{*m*}H[−] anion species, C₄H[−], C₆H[−], and C₈H[−], were found in IRC+10216 (McCarthy et al. 2006; Cernicharo et al. 2007; Kasai et al. 2007; Remijan et al. 2007). It was proposed that C_{*m*}H[−] is produced by an electron radiative attachment as follows:



The C_{*m*}H molecules have large electron affinities, and thus transformations to negative ion species by electron radiative attachment occur effectively, especially in longer ones (Herbst & Osamura 2008). The ratios of [C₄H[−]]/[C₄H], [C₆H[−]]/[C₆H], and [C₈H[−]]/[C₈H] in IRC+10216 were observed to be 2.4 × 10^{−4}, (6.2–8.6) × 10^{−2}, and (2.6–3.7) × 10^{−1}, respectively (Cernicharo et al. 2007; Kasai et al. 2007; Kawaguchi et al. 2007; Remijan et al. 2007). The rate coefficients of electron radiative attachment of C₄H, C₆H, and C₈H were reported to be 9 × 10^{−11} (T/300)^{−1/2}, 1.4 × 10^{−8} (T/300)^{−1/2}, and 2.5 × 10^{−8} (T/300)^{−1/2} cm³ s^{−1}, respectively, by Agúndez et al. (2008). The rate coefficient of C₄H is, however, about two orders of magnitude smaller than the theoretical value of 1.1 × 10^{−8} (T/300)^{−1/2} cm³ s^{−1} (Herbst & Osamura 2008). On the other hand, the rate coefficients of C₆H and C₈H agree well with the theoretical values of 6.2 × 10^{−8} (T/300)^{−1/2} and

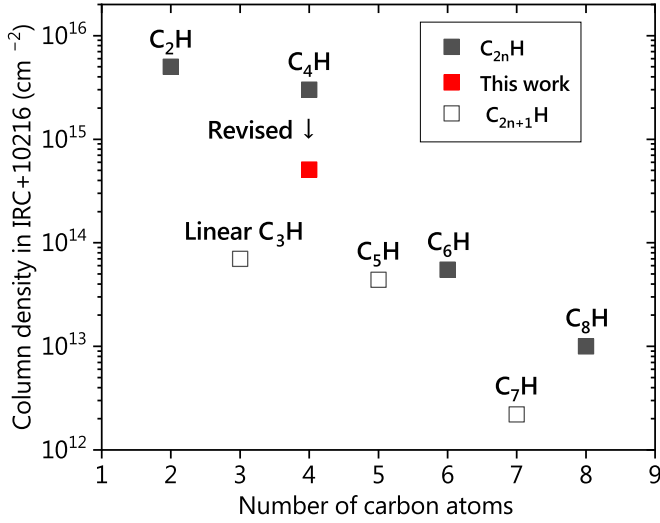


Figure 1. Column densities of $C_{2n}H$ and $C_{2n+1}H$ in the ground vibrational state in IRC+10216. The values from the previous work were taken from Cernicharo et al. (2000). Populations of these species are also partially distributed to the low-lying vibrationally excited states in this region (Cernicharo et al. 2000, Agúndez et al. 2017).

$6.2 \times 10^{-8} (T/300)^{-1/2} \text{ cm}^3 \text{ s}^{-1}$, respectively (Herbst & Osamura 2008). In short, the estimated rate coefficient of C_4H based on the reported column densities is abnormally small.

Similarly, molecular clouds show the discrepancy between the observed and theoretical values for the ratio of $[C_4H^-]/[C_4H]$. The observed values of this ratio in TMC-1 CP, the low-mass star-forming region L1527, and the photodissociation region Horsehead Nebula were reported to be $<5.2 \times 10^{-5}$, 1.1×10^{-4} , and $<3.3 \times 10^{-4}$, respectively (Agúndez et al. 2008), where the values in TMC-1 CP and Horsehead Nebula are 3σ upper limit. These ratios are two or three orders of magnitude smaller than the theoretical ratios of 7×10^{-3} , 8.5×10^{-2} , and 3.5×10^{-2} (Millar et al. 2007; Harada & Herbst 2008; Herbst & Osamura 2008).

Herbst & Osamura (2008) suggested that these inconsistencies between the observed and theoretical abundance ratios originated from the dipole moment of C_4H . By the quantum chemical calculations which have not included the effect of strong mixing of the electronic states, a small dipole moment is estimated for the electronic ground state of C_4H . For example, the dipole moment in the electronic ground state of $^2\Sigma^+$ was calculated to be 0.87 D (Woon 1995) by the restricted open-shell coupled cluster with single and double excitations and subsequent use of perturbation theory for triple excitations (RCCSD(T)) (Knowles et al. 1993; Deegan & Knowles 1994) with the augmented correlation-consistent valence double zeta (aug-cc-pVDZ) basis set (Dunning 1989; Kendall et al. 1992). In these calculations, C_4H was estimated to have a low-lying electronic excited state of $^2\Pi$ with the large dipole moment of 4.40 D, where the energy difference between the $^2\Sigma^+$ and $^2\Pi$ states was about 70 cm^{-1} (Woon 1995). Based on spectral analysis of the optical electronic transition, the $^2\Pi$ character in the ground state of $^2\Sigma^+$ was estimated to be about 40% (Hoshina et al. 1998), which might give rise to a much larger effective dipole moment than 0.87 D in the ground state.

In this work, the effective dipole moment in the ground state was calculated for the first time by quantum chemical calculations considering the mixing between the $^2\Sigma^+$ and $^2\Pi$ states. The column densities of C_4H in the dark clouds, the

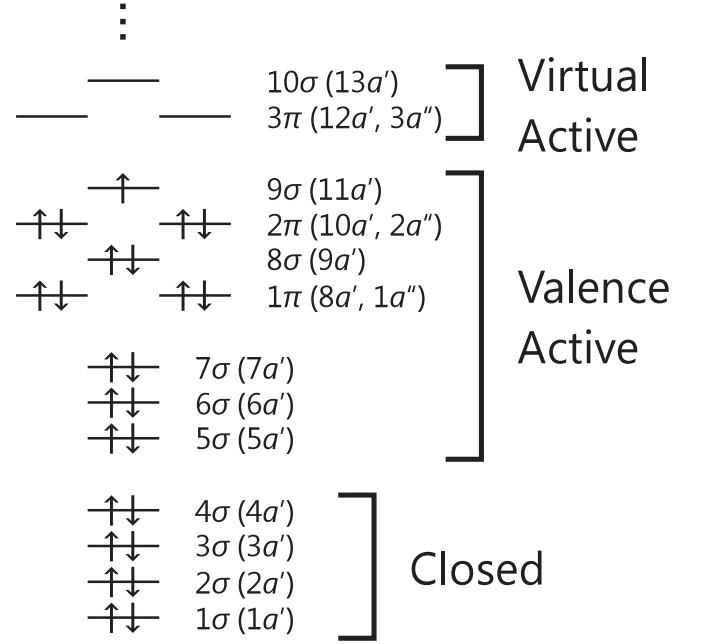


Figure 2. Molecular orbitals of C_4H and their symmetries at linear geometry. Labels in the parentheses denote symmetries at bent geometry in the C_s point group.

low-mass star-forming regions, and the circumstellar envelope IRC+10216 were reanalyzed using the new dipole moment.

2. Quantum Chemical Calculations

Quantum chemical calculations were performed using the MOLPRO 2012 package (Werner et al. 2012). To consider the mixing between the $^2\Sigma^+$ and the $^2\Pi$ states, we used the multireference configuration interaction (MRCI) method. The nine valence orbitals, $5\sigma (5a')$, $6\sigma (6a')$, $7\sigma (7a')$, $1\pi (8a', 1a'')$, $8\sigma (9a')$, $2\pi (10a', 2a'')$, and $9\sigma (11a')$, and the three virtual orbitals, $3\pi (12a', 3a'')$ and $10\sigma (13a')$, were considered as active orbitals as shown in Figure 2. The rest of the orbitals in the inner shell were closed. Geometrical optimization was performed by the MRCI method using the cc-pVQZ basis set. Although the previous RCCSD(T) calculations gave the linear structure in the $^2\Sigma^+$ ground state of C_4H as an optimized equilibrium structure (Woon 1995; Graf et al. 2001), the MRCI calculations derived a bent structure with an A' symmetry as shown in Figure 3. An effective dipole moment was calculated at the MRCI/cc-pVQZ level of theory. The dipole moment along the a -axis, μ_a , was obtained to be 2.10 D in the ground state, which is 2.4 times larger than the previous values (Woon 1995; Graf et al. 2001). The $^2\Pi$ character in the ground electronic state was estimated to be about 40%, which agrees with the reported value based on optical spectroscopy (Hoshina et al. 1998).

The bent structure for C_4H in this study corresponds to an equilibrium structure at the potential minimum. Then we examined the vibrational effect of the bending motion on the molecular structure. Potential energy curve (PEC) for the terminal $C_1-C_2-C_3$ angle of $C_1-C_2-C_3-C_4-H$ was calculated at the MRCI/cc-pVTZ level of theory as shown in Figure 4, where the $C_2-C_3-C_4$ and C_3-C_4-H angles were fixed at 180° and all of the bond lengths were optimized at the individual angles of 140° , 150° , 160° , 170° , and 180° for $C_1-C_2-C_3$. The values of individual points in this figure denote the dipole

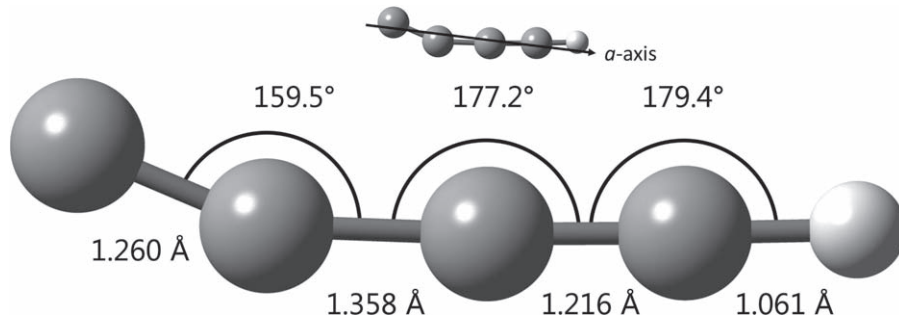


Figure 3. Equilibrium structure of C_4H in the electronic ground state of $^2A'$ by the quantum chemical calculation of MRCI/cc-pVQZ.

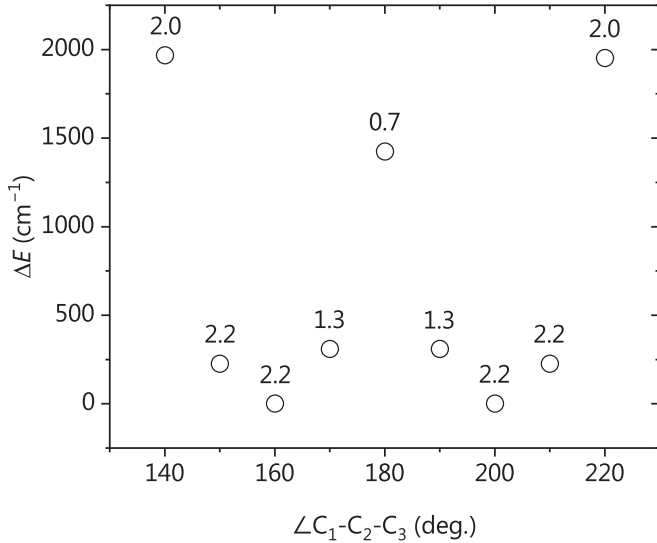


Figure 4. Potential energy curve of C_4H obtained by ab initio calculations at the MRCI/cc-pVTZ level of theory. The $C_2-C_3-C_4$ and C_3-C_4-H angles were fixed at 180° , and all of the bond lengths were optimized at the individual $C_1-C_2-C_3$ angles. The values of individual points denote the dipole moment along the a -axis in Debye. To execute multipoint calculations, the smaller basis function cc-pVTZ was utilized instead of cc-pVQZ. Although the dipole moment at the equilibrium structure, 2.2 D, is slightly larger than that by the cc-pVQZ basis function, 2.1 D, this difference is within the uncertainty of calculations.

moment along the a -axis in Debye. To speed up calculations of the PEC, the smaller basis function cc-pVTZ was used instead of cc-pVQZ. Despite of this speed up, cc-pVTZ can give us the comparable dipole moment of 2.2 D at the potential minimum with that obtained by cc-pVQZ, which shows the validity of cc-pVTZ. The PEC is slightly and clearly asymmetric based on the bond angles of 160° and 200° due to the finite potential barrier at 180° . The dipole moment clearly becomes smaller if the terminal $C_1-C_2-C_3$ angle approaches 180° from 160° . The terminal angle in the vibrationally averaged structure become slightly and clearly larger than the equilibrium value of 160° , as the PEC is slightly asymmetric. The mixing of the electronic states for this vibrationally averaged structure is slightly smaller than the one at the equilibrium position. Therefore, the effective dipole moment, μ_a , for the former structure would be slightly smaller than that for the latter one. The effects of zero-point vibrational motion to the terminal $C_1-C_2-C_3$ angle may be small, because the bending frequency on this angle is 179 cm^{-1} reported by Zhou et al. (2007), which is much smaller than the potential barrier between the two minima in Figure 4. The molecular structure of C_4H was discussed by McCarthy et al. (1995) based on the millimeter-wave rotational

Table 1
Calculated Structural Parameters of C_4H

Parameter	RCCSD(T)/129 cGTO ^a	MRCI/cc-pVQZ ^b	Exp. ^a
$r_{C_1C_2}$ (Å)	1.213(1)	1.260	1.224(3)
$r_{C_2C_3}$ (Å)	1.372(1)	1.358	1.359(3)
$r_{C_3C_4}$ (Å)	1.208(1)	1.216	1.215(3)
r_{C_4H} (Å)	1.062(1)	1.061	1.055(5)
$\angle C_1C_2C_3$ (deg.)	...	159.5	...
$\angle C_2C_3C_4$ (deg.)	...	177.2	...
$\angle C_3C_4H$ (deg.)	...	179.4	...

Notes.

^a McCarthy et al. (1995). A linear structure is assumed. The errors are 1σ .

^b Present study.

spectra for the normal species and its ^{13}C isotopomers. Assuming a linear structure of $C_1-C_2-C_3-C_4-H$, they derived the bond length of C_1-C_2 , C_2-C_3 , C_3-C_4 , and C_4-H to be 1.224(3), 1.359(3), 1.215(3), and 1.055(5) Å, respectively, where values in parentheses denote 1σ errors and apply to the last digits. The calculated bond lengths in the present study are 1.260, 1.358, 1.216, and 1.061 Å, which agree well with the experimental values except for the terminal C_1-C_2 bond, as shown in Table 1. The reason for the significantly short C_1-C_2 bond obtained by McCarthy et al. (1995) can be ascribed to the fact that the $C_1-C_2-C_3$ part is bent, in which the estimated bond length assuming a linear structure corresponds to a projection component of the true value of the C_1-C_2 bond. The rotational constant obtained from the equilibrium structure $\bar{B} = (B + C)/2$ was derived to be 4800 MHz by the present calculation, which agrees with the experimental value of 4758.65547(7) MHz (Gottlieb et al. 1983). Hence, considering this aspect, the assumption of a bent vibrationally averaged structure should be supported.

For C_4H , the ν_7 bending state in the $^2\Sigma^+$ electronic ground state is close to that in the $^2\Pi$ electronic excited state due to the bending frequency of 179 cm^{-1} (Zhou et al. 2007), giving a strong vibronic coupling between both states (Yamamoto et al. 1987). This coupling is included in the present MRCI calculations.

The interaction between the $^2\Sigma^+$ and the $^2\Pi$ states leading to a considerable increase of the dipole moment in the ground state may occur only for C_4H in the C_mH series, because C_4H is the unique molecule having a significantly small energy difference between these states. The energy differences between the $^2\Sigma^+$ and the $^2\Pi$ states, $E(^2\Pi) - E(^2\Sigma^+)$, for C_2H , C_4H , C_6H , and C_8H are experimentally estimated to be 3693, 222, -1412, and -2112 cm^{-1} , respectively (Garand et al. 2010;

Table 2
Column Densities and Rotational Temperatures of C₄H in Various Sources

Objects	Reported		Revised		Number of Fitted Lines ^a	Reference
	N (cm ⁻²)	T_{rot} (K)	N (cm ⁻²)	T_{rot} (K)		
L483	6.9×10^{13}	10	$1.8(3) \times 10^{13}$	7.9(8)	4	1, 2
TMC-1 CP	2.9×10^{14}	6.7	5.4×10^{13}	6.7 ^b	2	3
Barnard 1	2.5×10^{14}	5	4.6×10^{13}	5 ^b	2	1
L134N	6.1×10^{13}	5	1.1×10^{13}	5 ^b	2	1
Horsehead	3.0×10^{13}	15	5.5×10^{12}	15 ^b	2	1
Orion Bar	2.5×10^{13}	15	4.3×10^{12}	15 ^b	2	1
L1527	$1.01(5) \times 10^{14}$	14.3(13)	$3.01(10) \times 10^{13}$	14.4(9)	4	4
Lupus-1A	$5.0_{-2.0}^{+2.1} \times 10^{14}$	7.3	9.0×10^{13}	7.3 ^b	1	5
IRC+10216	3.0×10^{15}	35	5.1×10^{14}	35 ^b	... ^c	6

Notes.

^a Counting fine structure splitting lines.

^b Fixed.

^c Column density was simply calculated by multiplying the previous value by square of the ratio of the dipole moments, $(0.87/2.10)^2$.

References. (1) Agúndez et al. (2008), (2) present work, (3) Sakai et al. (2008), (4) Araki et al. (2012), (5) Sakai et al. (2010c), (6) Cernicharo et al. (2000).

Mazzotti et al. 2011; Sharp-Williams et al. 2011). Although the vibronic coupling between the $^2\Sigma^+$ and $^2\Pi$ states also occur for C₆H (Cernicharo et al. 2008), considerable changes of the dipole moment and column densities of the ground state may not occur because the energy difference of C₆H is not so small. As a result, the column densities of C₆H may not show abnormal values.

3. Results and Discussion

3.1. Reevaluation of Column Densities of C₄H

Using the effective dipole moment, reanalysis of the column densities of C₄H were carried out via intensities of rotational transitions assuming the local thermodynamic equilibrium (LTE) by the following formulae:

$$T_A^* = \eta_{\text{MB}} \{J(T_{\text{ex}}) - J(2.7)\} \{1 - \exp(-\tau)\}$$

where

$$J(T) = \frac{h\nu}{k} \left\{ \exp\left(\frac{h\nu}{kT}\right) - 1 \right\}^{-1}$$

and

$$\tau = \frac{8\pi^3}{3h\Delta\nu} \sqrt{\frac{4\ln 2}{\pi}} \frac{N}{Q} \mu^2 (J_{\text{low}} + 1) \times \exp\left\{-\frac{E_{\text{low}}}{kT_{\text{ex}}}\right\} \left\{1 - \exp\left(-\frac{h\nu}{kT_{\text{ex}}}\right)\right\} S_{\text{rel}}.$$

In the above formulae, T_A^* is the antenna temperature, η_{MB} is the main beam efficiency, T_{ex} is the excitation temperature, τ is the optical depth, ν is the transition frequency, $\Delta\nu$ is the line width (full width half maximum), N is the column density, Q is the partition function neglecting hyperfine structure, J_{low} is the rotational quantum number of the lower state, E_{low} is the energy level of the lower state, and S_{rel} is the relative intensity of each hyperfine component where a sum of these components in a rotational transition is 1. In the case of IRC+10216, a column density was simply recalculated by applying the square of the dipole moment ratio, $(0.87/2.10)^2$, to the previous value (Cernicharo et al. 2000), because line shapes in this region are not single Gaussian.

The column densities and the rotational temperatures of C₄H in the dark clouds, the low-mass star-forming regions, and the

circumstellar envelope are listed in Table 2. Adopting the new effective dipole moment, the revised column densities in all sources in Table 2 are about a factor of 6 smaller than the previous values.

3.2. Reevaluation of Abundance Anomaly of C₄H

The column densities of C_{*m*}H ($m=2-8$) in the ground vibrational state in IRC+10216 with respect to the number of carbon atoms are plotted in Figure 1. As mentioned in Section 1, the column density of C₄H, 3.0×10^{15} cm⁻², in the previous work is comparable with 5.0×10^{15} cm⁻² of C₂H and is about two orders of magnitude higher than 5.5×10^{13} cm⁻² of C₆H (Cernicharo et al. 2000). However, the revised column density of C₄H, 5.1×10^{14} cm⁻², marked by a red square is 1/9.8 of the reported value of C₂H and is 9.3 times larger than the reported value of C₆H. The column densities of C₂H, C₄H, C₆H, and C₈H decrease almost in an exponential manner along the numbers of carbon atoms, which apparently give rise to almost linear relations in Figure 1. The pumping mechanisms of C_{2*n*}H ($n=1-3$) to its vibrationally excited states in IRC+10216 was suggested by Agúndez et al. (2017). Populations of these species are partially distributed to the low-lying vibrationally excited states in this region. Although the column densities shown in Figure 1 may be slightly different from its total column densities, the linear relations do not change a lot in this log scale plot. Similar trends for linearity are also seen in the starless dark cloud TMC-1 CP, the low-mass star-forming region L1527, and the starless core Lupus-1A, as shown in Figure 5, despite of their different physical and chemical conditions. Hence, the exponential reductions for the column densities of C_{2*n*}H are ubiquitous in interstellar medium without any anomalous behavior along the number of carbon atoms. The effect of the possible difference of reactivity between C_{2*n*}H of $n=1$ and 2 with the $^2\Sigma^+$ ground state and C_{2*n*}H of $n=3$ and 4 with the $^2\Pi$ ground state, as mentioned in Section 1, is not seen in Figure 5.

Figure 6 shows the observed abundances of the C_{*m*}H molecules, including C_{2*n*}H and C_{2*n*+1}H, relative to the total hydrogen column density $N_{\text{H}} = 6 \times 10^{22}$ cm⁻² in L1527 (Jørgensen et al. 2002; Sakai et al. 2008, 2010a; Araki et al. 2012, 2017). The simulated ones in the cold and warm conditions at 10 and 30 K, respectively, are also shown in the

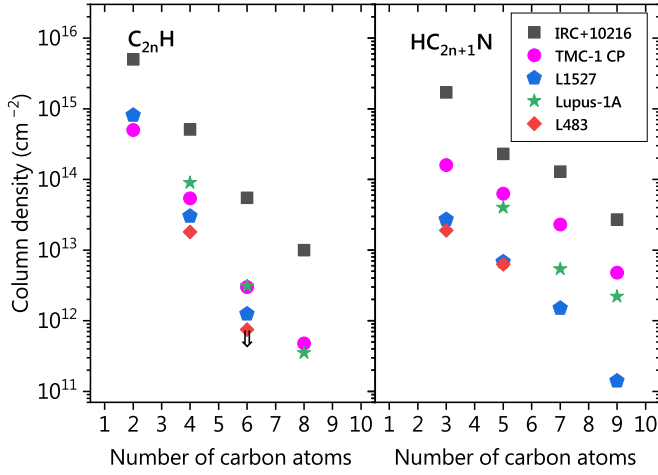


Figure 5. Column densities of $C_{2n}H$ and $HC_{2n+1}N$ in dark clouds, low-mass star-forming regions, and a circumstellar envelope IRC+10216. The values of C_4H are our revised values. Other values of the $C_{2n}H$ series are from Cernicharo et al. (2000) in IRC+10216; Liszt et al. (2018), Sakai et al. (2007, 2008), and Brünken et al. (2007) in TMC-1 CP; Sakai et al. (2008, 2010a) and Araki et al. (2012, 2017) in L1527; Sakai et al. (2010c) in Lupus-1A; and Agúndez et al. (2008) and the present work in L483. The value of C_6H in L483 is an upper limit. The values of the $HC_{2n+1}N$ series are from Kawaguchi et al. (1995) in IRC+10216; Takano et al. (1990, 1998) and Sakai et al. (2008) in TMC-1 CP; Sakai et al. (2008, 2009) in L1527; Sakai et al. (2010c) in Lupus-1A; and Hirota et al. (2009) and the present work in L483.

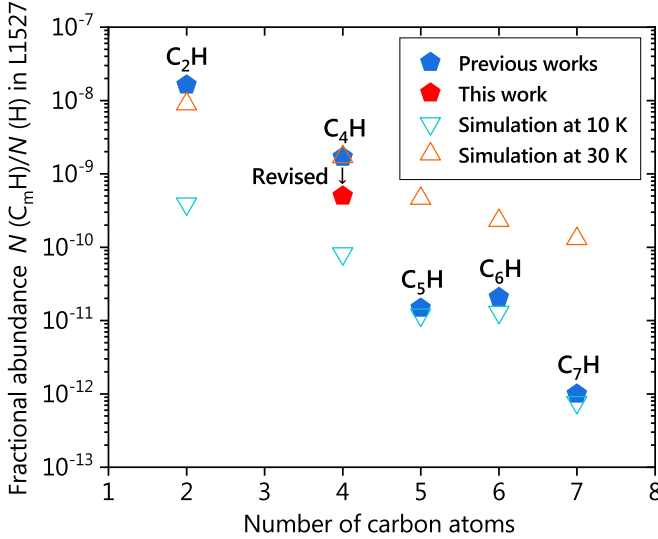


Figure 6. Fractional abundances of C_mH , including $C_{2n}H$ and $C_{2n+1}H$ in L1527. The column densities of C_2H , C_4H , and C_5H are from Sakai et al. (2010a), Araki et al. (2012), and Sakai et al. (2008), respectively. The values of C_6H and C_7H are from Araki et al. (2017). The total hydrogen column density N_H is assumed to be $6 \times 10^{22} \text{ cm}^{-2}$ (Jørgensen et al. 2002). The simulations of the fractional abundances in L1527 were reported by Hassel et al. (2008).

figure (Hassel et al. 2008). Araki et al. (2017) suggested that C_5H , C_6H , and C_7H are remnants of the early evolutionary phase of this molecular cloud. This is because the abundances of these molecules agree with the simulations in the cold condition although this cloud is warm at present. They also mentioned that C_4H was produced by warm carbon-chain chemistry (WCCC), because the amount of C_4H agrees with the simulation in the warm condition. However, since the revised amount of C_4H is in between the cold and the warm cases, the contribution of WCCC in the formation of C_4H may be smaller than that considered in the previous study.

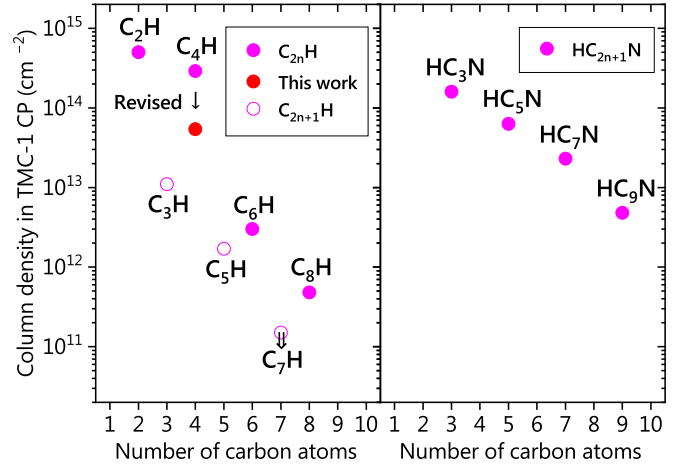


Figure 7. Column densities of C_mH including $C_{2n}H$ and $C_{2n+1}H$, and $HC_{2n+1}N$ molecules in TMC-1 CP. The values of C_2H and C_3H are from Liszt et al. (2018), where the value of C_3H is the sum of the values for the cyclic and linear conformers. The values of C_4H , C_5H , and C_6H are from Sakai et al. (2007, 2008). The value of C_7H is an upper limit from Bell et al. (1999). The value of C_8H is from Brünken et al. (2007). The values of HC_3N and HC_5N are from Takano et al. (1990, 1998). The values of HC_7N and HC_9N are from Sakai et al. (2008).

The column densities of C_mH , including $C_{2n}H$ and $C_{2n+1}H$, and $HC_{2n+1}N$ in TMC-1 CP are shown in Figure 7. Generally, $C_{2n+1}H$ and $HC_{2n+1}N$ series show a linear relation. The $C_{2n}H$ series also shows a linear relation after the current revision. Carbon-chain extension mechanisms of the $C_{2n}H$ and $C_{2n+1}H$ series may be similar, because the trends of both series are similar to each other. Three cases of extension mechanisms for the C_mH series are considered: (1) one by one, i.e., both $C_{2n}H$ and $C_{2n+1}H$ belong to one series (Suzuki 1983), (2) two by two (Mitchell et al. 1979; Schiff & Bohme 1979), i.e., $C_{2n}H$ and $C_{2n+1}H$ are independent series of each other, and (3) all C_mH molecules are individually formed, which is inferred from the discussion for the formation mechanism of $HC_{2n+1}N$ (See below). Linearities of $C_{2n}H$ and $C_{2n+1}H$ seem to exclude the case of (3). However, a linearity does not always suggest the formation mechanism of the cases of (1) or (2). For example, linearities are also seen in the $HC_{2n+1}N$ molecules (Figure 5), although the $HC_{2n+1}N$ series except HC_3N were mainly formed not by two by two such as $HC_{2n+1}N + C_2H_2^+$ but by individual formation such as $C_{2n+1}H_m^+ (m = 3-5) + N$ in TMC-1 CP (Taniguchi et al. 2016; Burkhardt et al. 2018).

Sakai et al. (2010b, 2013) observed the ^{13}C isotopomers of C_2H and C_4H in TMC-1 CP. The abundance ratios of $[CCH]/[C^{13}CH]$ and $[CCH]/[^{13}CCH]$ are larger than 170 and 250, respectively. Two carbon atoms of C_2H are inequivalent, suggesting that the $C + CH_2$ reaction contributes to the production of C_2H (Sakai et al. 2010b). On the other hand, the ratios of $[C_4H]/[^{13}CCCCH]$, $[C_4H]/[C^{13}CCCH]$, $[C_4H]/[CC^{13}CCH]$, and $[C_4H]/[CCC^{13}CH]$ are 141(44), 97(27), 82(15), and 118(23), respectively (Sakai et al. 2013). The inner two carbon atoms and the outer two atoms of C_4H are inequivalent, suggesting that the $C_4H_2^+ + e^-$ reaction contributes to the production of C_4H (Sakai et al. 2013). As shown above, the formation mechanisms of $C_{2n}H$ and $HC_{2n+1}N$, may be different between the shortest species and longer ones. Based on the linear relation and the similarity between $C_{2n}H$ and $HC_{2n+1}N$, the $C_{2n}H$ series except C_2H are thought to be systematically formed from the similar chemical species such as $XC_{2n}Y$ or $XC_{2n}Y^+$ series, where each of X and

Y indicates an arbitrary atom or substituent except for a carbon atom.

In summary, the simple linear relation of the column densities for the $C_{2n}H$ series in these various sources suggests high similarities among the formation mechanisms of these species.

3.3. Reevaluation of $[C_4H^-]/[C_4H]$ Ratios and Electron Radiative Attachment Rate Coefficients of C_4H

The C_mH molecules have large electron affinities, and thus transformations to negative ion species by electron radiative attachment occur effectively. The $[C_4H^-]/[C_4H]$ ratio in IRC+10216 is revised to be 1.4×10^{-3} from the previous ratio of 2.4×10^{-4} (Cernicharo et al. 2007) by our new dipole moment. Thus, the electron radiative attachment rate coefficient of C_4H is revised to be $5 \times 10^{-10} (T/300)^{-1/2} \text{ cm}^3 \text{ s}^{-1}$ from the previous rate coefficient of $9 \times 10^{-11} (T/300)^{-1/2} \text{ cm}^3 \text{ s}^{-1}$ (Agúndez et al. 2008), where an electron radiative attachment rate coefficient is assumed to be simply proportional to the $[C_4H^-]/[C_4H]$ ratio (Formula 3 of Cernicharo et al. 2007). The revised rate coefficient falls within about one order of magnitude of the theoretical rate coefficient of $1.1 \times 10^{-8} (T/300)^{-1/2} \text{ cm}^3 \text{ s}^{-1}$ (Herbst & Osamura 2008). The difference between the observational and calculated value is greatly reduced.

In addition to IRC+10216, the $[C_4H^-]/[C_4H]$ ratios in TMC-1 CP, L1527, and Horsehead Nebula are revised to be $<3.0 \times 10^{-4}$, 6.4×10^{-4} , and $<1.9 \times 10^{-3}$, respectively. The revised ratios are approached to the theoretical ratios of 7×10^{-3} , 8.4×10^{-2} , and 3.5×10^{-2} (Millar et al. 2007; Harada & Herbst 2008; Herbst & Osamura 2008), although they are still one or two orders of magnitude smaller.

Herbst & Osamura (2008) suggested that if C_4H has a large dipole moment of >2 D, this molecule forms a weak-bound complex with an electron, i.e., a dipole-bound state. This will complicate the simulation of electron radiative attachment of C_4H , because C_4H effectively accesses thermal electrons. The accurate evaluation of amounts of C_4H may be carried out by considering the influence of the weak-bound complex.

3.4. Other Influences by Reevaluation of Dipole Moment of C_4H

The present reevaluation of the dipole moment of C_4H means larger Einstein's A coefficients for individual rotational transitions. Thus, we expect (1) larger critical densities and (2) deviation from LTE. Concerning the first point, for example, mappings using high- N emission of C_4H (e.g., Agúndez et al. 2017) need to be modified as tracings of higher density regions in clouds, because the critical densities of C_4H are a factor of 6 larger than the previously estimated values. Stronger radiational cooling causes its lower rotational temperature under the LTE approximation.

3.5. Mixing of Electronic States of C_5N

Aside from C_4H , some interstellar molecules having two different electronic states very close in energy can show remarkably large or small column densities. One of the examples is C_5N . The C_3N/C_5N ratios are one order of magnitude larger than those of HC_3N/HC_5N in IRC+10216 and TMC-1 (Guélin et al. 1998), and the C_5N/C_5N^- ratio is

only 1.8 in IRC+10216 (Cernicharo et al. 2008). These abnormal ratios are thought to be due to an underestimate of the column densities of C_5N by the overestimate of a dipole moment of C_5N . Without consideration of the mixing between two electronic states, the dipole moment of C_5N in the electronic ground state of $^2\Sigma^+$ was calculated to be 3.385 D by RCCSD(T) with 204 contracted Gaussian-type orbitals (204 cGTOs) (Botschwina 1996). The first electronic excited state of $^2\Pi$ lies 560 (120) cm^{-1} above the ground state (Yen et al. 2010). We calculated the dipole moment of the $^2\Pi$ state to be 0.569 D at the RCCSD(T)/cc-pVTZ level of theory without considerations of the mixing for both of the states. However, these states could be mixed with each other because their energy difference is small. Therefore, the effective dipole moment of C_5N in the ground state could be smaller than 3.385 D, and the actual column densities of C_5N are larger than the reported values, i.e., the present column densities can be modified. As a result, the C_3N/C_5N and C_5N/C_5N^- ratios become smaller and larger than the previous values, respectively. The detailed calculations will be presented in a separated paper.

3.6. Abundance of Carbon-chain Molecules in L483

The decreasing trends of the $C_{2n}H$ and $C_{2n+1}H$ series with carbon-chain length are definitely more prominent than that of the $HC_{2n+1}N$ series in TMC-1 CP as shown in Figure 7. These trends are also seen in IRC+10216, L1527, and Lupus-1A (Figure 5). It is interesting to know that such a tendency is also seen to the low-mass star-forming region L483 where both WCCC and hot corino chemistry (HCC) work (Oya et al. 2017). However, the data for carbon-chain molecules are not enough to unveil the contributions of WCCC and HCC for chemical composition in this region. In the present study, the column densities and the rotational temperatures of C_4H , HC_3N , and HC_5N are derived through the analysis of their rotational lines, and an upper limit of the column density of C_6H are also estimated. These data for L483 are compared with those for TMC-1 CP, IRC+10216, L1527, and Lupus-1A.

The observational conditions were as follows. We carried out observations toward L483 ($18^h17^m29^s.8$, $-04^\circ39'38''.3$, J2000) by using the 45 m telescope of Nobeyama Radio Observatory in 2018 March 29–31. The T70 receiver was used to observe the carbon-chain molecules, C_4H , C_6H , HC_3N , and HC_5N in the 76.10–77.23 and 88.15–90.61 GHz regions, where signals with two linear polarizations were averaged. The SAM45 spectrometer was set as the spectral resolution of 15.26 kHz, which corresponds to the velocity resolution of 0.05–0.06 km s^{-1} in 90.6–76.1 GHz. The beamwidth was $19''.0$ – $20''.3$, and the main beam efficiency was 0.55. The beam filling factor was assumed to be 1. The effective integration times (on-source times) were about 5 hr, and a root mean square (rms) of noise was achieved to be 34 mK in T_B .

3.6.1. C_4H

The $N = 8$ –7 transition of C_4H was observed as shown in Table 3 and Figure 8. Using the revised dipole moment, a least-squares analysis was carried out for this and the reported $N = 9$ –8 transitions (Agúndez et al. 2008). The column density and the rotational temperature of C_4H are derived to be $1.8(3) \times 10^{13} \text{ cm}^{-2}$ and 7.9(8) K, respectively (Table 2), where

Table 3
Observed Transitions of C₄H in L483

Transition	Frequency ^a (MHz)	T_A^* (K)	$\Delta\nu$ (km s ⁻¹)	η_{MB}	Reference
$N = 8-7 \ J = 8.5-7.5$	76117.43	0.548(14)	0.364(11)	0.55	1
$N = 8-7 \ J = 7.5-6.5$	76156.02	0.487(14)	0.369(12)	0.55	1
$N = 9-8 \ J = 9.5-8.5$	85634.00	0.387(15)	0.60(6)	0.82	2
$N = 9-8 \ J = 8.5-7.5$	85672.57	0.332(15)	0.70(6)	0.82	2

Note.

^a Gottlieb et al. (1983).

References. (1) Present work; (2) Agúndez et al. (2008).

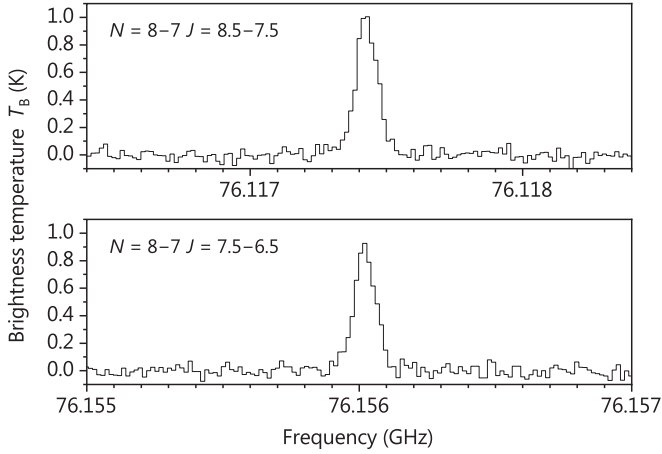


Figure 8. Observed $N = 8-7$ transition of C₄H in L483.

the errors are 1σ . The column density is plotted in Figure 5 (left panel). The column density is about one-fourth of the reported value of $6.9 \times 10^{13} \text{ cm}^{-2}$ (Agúndez et al. 2008), because the smaller dipole moment of 0.87 D and the slightly higher rotational temperature of 10 K were assumed in the previous analysis. If the temperature of 10 K is assumed in this work, the column density is calculated to be $1.3 \times 10^{13} \text{ cm}^{-2}$.

3.6.2. C₆H

Since we could not detect the $J = 27.5-26.5$ transition ($\Omega = 3/2$, e and f, 76234.155 and 76254.587 MHz) of C₆H (Linnartz et al. 1999), we estimated the upper limit of its column density to be $7.5 \times 10^{11} \text{ cm}^{-2}$ (see the left panel in Figure 5), under the assumption that (1) the maximum peak intensity of this transition is smaller than three times rms of noise and (2) the rotational temperature of C₆H is fixed to the kinetic temperature of L483 as 10 K (Tafalla et al. 2000).

Assuming the same slope for L483 as the low-mass star-forming region L1527 in Figure 5, the column densities of C₂H and C₆H in L483 are estimated to be 5×10^{14} and $7 \times 10^{11} \text{ cm}^{-2}$, respectively. The estimated value of C₆H is close to the obtained upper limit in the present study.

3.6.3. HC₃N

The $J = 10-9$ transition of HC₃N was observed as listed in Table 4. Using this and the reported $J = 5-4$ transitions (Hirota et al. 2009), the column density and the rotational temperature of HC₃N are derived to be $1.9 \times 10^{13} \text{ cm}^{-2}$ and 10.9 K, respectively. The column density is plotted in Figure 5 (right panel). This column density is about 1/1.6 of the reported

Table 4
Observed Transitions of HC₃N, H¹³CCCN, HC¹³CCN, and HCC¹³CN in L483

Transition	Frequency ^a (MHz)	T_A^* (K)	$\Delta\nu$ (km s ⁻¹)	η_{MB}	Reference
HC ₃ N					
$J = 5-4$	45490.307	2.03(18)	0.85(9)	0.7	1
$J = 10-9$	90979.023	1.93(5)	0.565(17)	0.55	2
H ¹³ CCCN					
$J = 10-9$	88166.832	0.044(11)	0.49(14)	0.55	2
HC ¹³ CCN					
$J = 10-9$	90593.059	0.061(7)	0.59(8)	0.55	2
HCC ¹³ CN					
$J = 10-9$	90601.777	0.084(10)	0.32(5) ^b	0.55	2

Notes.

^a Creswell & Winnewisser (1977).

^b Possibly partially blended line.

References. (1) Hirota et al. (2009), (2) present work.

Table 5
Observed Transitions of HC₅N in L483

Transition	Frequency ^a (MHz)	T_A^* (K)	$\Delta\nu$ (km s ⁻¹)	η_{MB}	Reference
$J = 17-16$	45264.720	0.75(21)	0.40(14)	0.7	1
$J = 29-28$	77214.359	0.063(6)	0.66(7)	0.55	2

Note.

^a Bizzocchi et al. (2004).

References. (1) Hirota et al. (2009), (2) present work.

value of $3.1 \times 10^{13} \text{ cm}^{-2}$ (Hirota et al. 2009), because the slightly smaller rotational temperature of 6.5 K is assumed in the previous study.

In addition, the $J = 10-9$ transitions of the ¹³C isotopomers of HC₃N were observed as listed in Table 4. The column densities of H¹³CCCN, HC¹³CCN, and HCC¹³CN are obtained to be $2.9(5) \times 10^{11}$, $4.8(9) \times 10^{11}$, and $3.6(5) \times 10^{11} \text{ cm}^{-2}$, respectively, where the errors are 1σ . The rotational temperature is assumed to be that of the normal species. Unfortunately, the signal-to-noise ratios of 3–5 obtained in our observations are insufficient to discuss formation mechanisms of HC₃N in L483 in detail as already done in L1527 (e.g., Araki et al. 2016).

3.6.4. HC₅N

The $J = 29-28$ transition of HC₅N was observed as shown in Table 5. Using this and the reported $J = 17-16$ transitions (Hirota et al. 2009), the column density and the rotational

temperature of HC_5N are estimated to be $6.3 \times 10^{12} \text{ cm}^{-2}$ and 12.4 K, respectively. The column density is plotted in Figure 5 (right panel). This column density is about one-third of the reported value of $1.8 \times 10^{13} \text{ cm}^{-2}$ (Hirota et al. 2009), because the smaller rotational temperature of 6.5 K is assumed in the previous study. If the temperature of 10 K is assumed, the column density is calculated to be $8.0 \times 10^{12} \text{ cm}^{-2}$.

From the above observation, it was confirmed that a decreasing trend of the C_{2n}H series is more prominent than that of the HC_{2n+1}N series also in L483.

4. Summary

The quantum chemical calculations were carried out in order to evaluate effective dipole moment of C_4H in its electronically ground state by using the MRCI method considering the mixing between the ground state of $^2\Sigma^+$ and the low-lying electronic excited state of $^2\Pi$ with the large dipole moment. As a result, the electronic ground state is $^2A'$, and its optimized equilibrium structure is bent. The effective dipole moment was derived to be 2.10 D, which is about 2.4 times larger than the value used so far. The column densities of C_4H in the dark clouds, the low-mass star-forming regions, and the circumstellar envelope were revised using this dipole moment. Obtained column densities are about a factor of 6 smaller than those in the previous studies. The column densities of the C_{2n}H ($n=1-4$) molecules in the various sources show the trends of simple exponential decays with the carbon-chain length without any anomalous variation between adjacent species. The trends suggest high similarities among formation mechanisms of C_{2n}H molecular series. Since the issues of C_4H are resolved, henceforth, the C_{2n}H molecules can be appropriately used to study models of chemical reaction networks for interstellar medium.

We thank the staff of Nobeyama Radio Observatory for their help with the observations. We are grateful to the anonymous reviewers for their valuable comments.

ORCID iDs

Takahiro Oyama  <https://orcid.org/0000-0002-2301-7951>

Mitsunori Araki  <https://orcid.org/0000-0003-4530-9741>

Shuro Takano  <https://orcid.org/0000-0001-6788-7230>

References

- Agúndez, M., Cernicharo, J., Guélin, M., et al. 2008, *A&A*, **478**, L19
 Agúndez, M., Cernicharo, J., Quintana-Lacaci, G., et al. 2017, *A&A*, **601**, A4
 Araki, M., Takano, S., Sakai, N., et al. 2016, *ApJ*, **833**, 291
 Araki, M., Takano, S., Sakai, N., et al. 2017, *ApJ*, **847**, 51
 Araki, M., Takano, S., Yamabe, H., et al. 2012, *ApJ*, **744**, 163
 Bell, M. B., Feldman, P. A., Watson, J. K. G., et al. 1999, *ApJ*, **518**, 740
 Bizzocchi, L., Degli, C., & Botschwina, P. 2004, *JMoSp*, **225**, 145
 Botschwina, P. 1996, *CPL*, **259**, 627
 Brünken, S., Gupta, H., Gottlieb, C. A., McCarthy, M. C., & Thaddeus, P. 2007, *ApJL*, **664**, L43
 Burkhardt, A. M., Herbst, E., Kalenskii, S. V., et al. 2018, *MNRAS*, **474**, 5068
 Canosa, A., Páramo, A., Picard, S. D. L., & Sims, L. R. 2007, *Icar*, **187**, 558
 Cernicharo, J., Guélin, M., Agúndez, M., et al. 2007, *A&A*, **467**, L37
 Cernicharo, J., Guélin, M., Agúndez, M., et al. 2008, *ApJL*, **688**, L83
 Cernicharo, J., Guélin, M., & Kahane, C. 2000, *A&AS*, **142**, 181
 Cernicharo, J., Guélin, M., Menten, K. M., & Walmsley, C. M. 1987, *A&A*, **181**, L1
 Creswell, R. A., & Winnewisser, G. 1977, *JMoSp*, **65**, 420
 Deegan, M. J. O., & Knowles, P. J. 1994, *CPL*, **227**, 321
 Dunning, T. H., Jr. 1989, *JChPh*, **90**, 1007
 Garand, E., Yacovitch, T. I., Sheehan, S. M., & Neumark, D. M. 2010, *Chem. Sci.*, **1**, 192
 Gottlieb, C. A., Gottlieb, E. W., & Thaddeus, P. 1983, *ApJ*, **275**, 916
 Graf, S., Geiss, J., & Leutwyler, S. 2001, *JChPh*, **114**, 4542
 Guélin, M., Neininger, N., & Cernicharo, J. 1998, *A&A*, **335**, L1
 Harada, N., & Herbst, E. 2008, *ApJ*, **685**, 272
 Hasegawa, T. I., Herbst, E., & Leung, C. M. 1992, *ApJS*, **82**, 167
 Hassel, G. E., Herbst, E., & Garrod, R. T. 2008, *ApJ*, **681**, 1385
 Herbst, E., & Leung, C. M. 1989, *ApJS*, **69**, 271
 Herbst, E., & Osamura, Y. 2008, *ApJ*, **679**, 1670
 Hirota, T., Ohishi, M., & Yamamoto, S. 2009, *ApJ*, **699**, 585
 Hoshina, K., Kohguchi, H., Ohshima, Y., & Endo, Y. 1998, *JChPh*, **108**, 3465
 Jørgensen, J. K., Schöier, F. L., & van Dishoeck, E. F. 2002, *A&A*, **389**, 908
 Kasai, Y., Kagi, E., & Kawaguchi, K. 2007, *ApJL*, **661**, L61
 Kawaguchi, K., Fujimori, R., Aimi, S., et al. 2007, *PASJ*, **59**, L47
 Kawaguchi, K., Kasai, Y., Ishikawa, S., & Kaifu, N. 1995, *PASJ*, **47**, 853
 Kendall, R. A., Dunning, T. H., Jr., & Harrison, R. J. 1992, *JChPh*, **96**, 6796
 Knowles, P. J., Hampel, C., & Werner, H.-J. 1993, *JChPh*, **99**, 5219
 Linnartz, H., Motylewski, T., Vaizert, O., et al. 1999, *JMoSp*, **197**, 1
 Liszt, H., Gerin, M., Beasley, A., & Pety, J. 2018, *ApJ*, **856**, 151
 Mazzotti, F. J., Raghunandan, R., Esmail, A. M., Tulej, M., & Maier, J. P. 2011, *JChPh*, **134**, 164303
 McCarthy, C. M., Gottlieb, C. A., Gupta, H., & Thaddeus, P. 2006, *ApJL*, **652**, L141
 McCarthy, C. M., Gottlieb, C. A., Thaddeus, P., Horn, M., & Botschwina, P. 1995, *JChPh*, **103**, 7820
 Millar, T. J., Walsh, C., Cordiner, M. A., Chuimin, R. N., & Herbst, E. 2007, *ApJL*, **662**, L87
 Mitchell, G. F., Huntress, W. T., Jr., & Prasad, S. S. 1979, *ApJ*, **233**, 102
 MOLPRO 2012, version 2012.1, a package of ab initio programs, ed. H.-J. Werner et al. see: <http://www.molpro.net>
 Oya, Y., Sakai, N., Watanabe, Y., et al. 2017, *ApJ*, **837**, 174
 Remijan, A. J., Hollis, J. M., Lovas, F. J., et al. 2007, *ApJL*, **664**, L47
 Saito, S., Kawaguchi, K., Suzuki, H., et al. 1987, *PASJ*, **39**, 193
 Sakai, N., Ikeda, M., Morita, M., et al. 2007, *ApJ*, **663**, 1174
 Sakai, N., Sakai, T., Hirota, T., & Yamamoto, S. 2008, *ApJ*, **672**, 371
 Sakai, N., Sakai, T., Hirota, T., & Yamamoto, S. 2009, *ApJ*, **702**, 1025
 Sakai, N., Sakai, T., Hirota, T., & Yamamoto, S. 2010a, *ApJ*, **722**, 1633
 Sakai, N., Saruwatari, O., Sakai, T., Takano, S., & Yamamoto, S. 2010b, *A&A*, **512**, A31
 Sakai, N., Shiino, T., Hirota, T., Sakai, T., & Yamamoto, S. 2010c, *ApJL*, **718**, L49
 Sakai, N., Takano, S., Sakai, T., et al. 2013, *JPCA*, **117**, 9831
 Schiff, H. I., & Bohme, D. K. 1979, *ApJ*, **232**, 740
 Sharp-Williams, E. N., Roberts, M. A., & Nesbitt, D. J. 2011, *JChPh*, **134**, 064314
 Smith, I. W. M., Herbst, E., & Chang, Q. 2004, *MNRAS*, **350**, 323
 Suzuki, H. 1983, *ApJ*, **272**, 579
 Suzuki, H., Ohishi, M., Kaifu, N., et al. 1986, *PASJ*, **38**, 911
 Tafalla, M., Myers, P. C., Mardones, D., & Bachiller, R. 2000, *A&A*, **359**, 967
 Takano, S., Masuda, A., Hirahara, Y., et al. 1998, *A&A*, **329**, 1156
 Takano, S., Suzuki, H., & Ohishi, M. 1990, *ApJL*, **361**, L15
 Taniguchi, K., Ozeki, H., Saito, M., et al. 2016, *ApJ*, **817**, 147
 Werner, H.-J., Knowles, P. J., Knizia, G., Manby, F. R., & Schütz, M. 2012, *WIREs Comput. Mol. Sci.*, **2**, 242
 Woon, D. E. 1995, *CPL*, **244**, 45
 Yamamoto, S., Saito, S., Guélin, M., et al. 1987, *ApJL*, **323**, L149
 Yen, T. A., Garand, E., Shreve, A. T., et al. 2010, *JPCA*, **114**, 3215
 Zhou, J., Garand, E., & Neumark, D. M. 2007, *JChPh*, **127**, 154320